Journal of Power Sources 215 (2012) 312–316

Contents lists available at SciVerse ScienceDirect

Journal of Power Sources

journal homepage: www.elsevier.com/locate/jpowsour

Short communication

Failure mechanisms of $LiNi_{0.5}Mn_{1.5}O_4$ electrode at elevated temperature

Taeho Yoon [b], Sangjin Park [b], Junyoung Mun [b], Ji Heon Ryu [b], Wonchang Choi [a], Yoon-Sok Kang [a], Jin-Hwan Park [a], Seung M. Oh [b,*]

[a] Battery Group, Energy Lab, SAIT (Samsung Advanced Institute of Technology), Yongin 446-712, Republic of Korea
[b] Department of Chemical and Biological Engineering, Institute for Chemical Processes, and WCU program of C2E2, Seoul National University, Seoul 151-744, Republic of Korea

HIGHLIGHTS

- Failure mechanisms in the $LiNi_{0.5}Mn_{1.5}O_4$ electrode at elevated temperature.
- The electrode failure is caused by the breakdown of electrically conductive network.
- Crack or void forms inside the composite electrode layer.
- Reinforcing the electrically conductive network is effective to mitigate the failure.

ARTICLE INFO

Article history:
Received 13 February 2012
Received in revised form
25 April 2012
Accepted 27 April 2012
Available online 8 May 2012

Keywords:
Li-ion batteries
Failure mechanism
High-voltage positive electrodes
Spinel
High-temperature electrode performances

ABSTRACT

Failure mechanisms involved in the high-voltage $LiNi_{0.5}Mn_{1.5}O_4$ electrode are studied at an elevated temperature (60 °C). At ambient temperature (25 °C), this oxygen-deficient spinel-structured electrode shows a reasonable cycle performance, but a rapid capacity decay after 40 cycles at 60 °C. An increase of electrode polarization and formation of electrically isolated active material, both of which become prominent from the 40th cycle, suggest that the electrode failure is mainly caused by the breakdown of electrically conductive network that is made between the active material, carbon and current collector in the composite electrode. The post-mortem electron microscope study reveals a crack formation at the electrode layer/aluminum current collector interface as well as inside the composite electrode layer, which can account for the electrode polarization and electrical isolation. The failure can, however, be mitigated by increasing the load of conductive carbon or polymeric binder, and also by using an etched aluminum foil as the current collector. All these countermeasures seem to be beneficial to reinforce the electrically conductive network.

1. Introduction

As an effort to increase the energy density of lithium secondary batteries, a few high-voltage positive electrode materials have been developed. One of the spotlighted materials is the lithium-excess layered oxide, $xLi_2MnO_3 \cdot (1-x)LiMO_2$ (M = Co, Ni, Mn), which has a higher working voltage and larger specific capacity than those of $LiCoO_2$ and $LiMn_2O_4$ [1–3]. The intrinsic problem for this material is, however, the structural change upon cycling from the layered to spinel phase, which is undesirable since it lowers the working voltage [2,3] Moreover, this material is unstable as the Mn^{3+} ions are prone to the disproportionation reaction and Jahn-Teller distortion [4].

The spinel-structured $LiNi_{0.5}Mn_{1.5}O_4$ (LNMO, hereafter) is also categorized as the high-voltage positive electrode material since its working voltage is as high as 4.6–4.8 V (*vs.* Li/Li^+). In this Ni-doped Mn spinel, only the nickel ions are redox active while the Mn ions are idling [5–7]. Namely, the two-electron redox reaction ($Ni^{2+} \leftrightarrow Ni^{4+}$) is responsible for the high-voltage charge/discharge reaction. This feature is contrasted by the un-doped Mn spinel ($LiMn_2O_4$), in which the charge/discharge reaction near 4.0 V is associated with the one-electron redox reaction by the Mn ions ($Mn^{3+} \leftrightarrow Mn^{4+}$). It is known that the un-doped spinel suffers from the structural degradations such as disproportionation reaction and Jahn-Teller distortion, which are caused by the formation of Mn^{3+} ions in the discharging period [4,8,9]. LNMO is free from such a structural degradation since the Mn valence is maintained at 4+. The high working voltage with an outstanding structural stability must be beneficial for the practical application of this material. This advantage is, however, largely offset by the instability of the cell

* Corresponding author. Tel.: +82 2 880 7074; fax: +82 2 872 5755.
E-mail address: seungoh@snu.ac.kr (S.M. Oh).

0378-7753/$ – see front matter © 2012 Elsevier B.V. All rights reserved.
doi:10.1016/j.jpowsour.2012.04.103

constituents, which is caused by the high working voltage. That is, at such a high charge/discharge potential, the electrolyte, polymeric binder, conductive carbon, aluminum current collector, and active material itself are not stable against oxidation, which is even more serious at elevated temperatures [10–13]. The degradation mechanisms of LNMO have been proposed in the literature, in which the metal dissolution by hydrogen fluoride attack [10] and electrode polarization due to a formation of surface film [14,15] have been proposed.

This work is an extension of the previous ones, in which the failure mechanism of LNMO is studied at an even harsher condition (elevated temperature). The dominant failure mechanism has been isolated among the possible ones such as metal dissolution, phase transition to inactive phases, electrical isolation of active components, and breakdown of electrically conductive network. Also, the countermeasures to mitigate the electrode failure are provided.

2. Experimental

The used LNMO powder was purchased from Tanaka Chem. Corp., Japan. A composite positive electrode was prepared by spreading the slurry of LNMO powder, Denka black (as a carbon additive for electrode conductivity enhancement), and poly(-vinylidene fluoride) (PVdF, Solef 620 as a polymeric binder) (94:3:3 in wt. % unless otherwise specified) on a piece of aluminum foil (as a current collector), which was followed by drying at 120 °C under vacuum for 12 h. The electrode was then pressed to enhance the inter-particle contact and to ensure better adhesion to the current collector. The used electrolyte was 1.3 *M* $LiPF_6$ dissolved in a mixture of ethylene carbonate (EC), diethyl carbonate (DEC) and ethylmethyl carbonate (EMC) (3:5:2 in vol. ratio). Coin-type cells (CR2032) were assembled with a lithium metal counter electrode and a poly propylene (PP) separator. The galvanostatic charge/discharge cycling was made using a Toscat-2100 cycler over the potential range of 3.5–4.9 V (*vs.* Li/Li^+). For complete charging, additional constant-voltage step was added at 4.9 V.

For a post-mortem X-ray diffraction (XRD) and field-emission scanning electron microscope (FE-SEM) analysis, the cycled cells were disassembled in an argon-filled glove box, and the LNMO electrodes were collected in their discharged state and washed with dimethyl carbonate (DMC). The XRD analysis was made using a D8-Brucker diffractometer equipped with Cu Ka radiation (1.54056 Å). To obtain the cross-sectional FE-SEM (Model JSM-6700F, JEOL) images, the electrode samples were crosscut by using an argon-ion beam polisher (SM-09010, JEOL) at a constant power of 0.5 W (5 kV and 0.1 mA) under vacuum ($<2.0 \times 10^{-4}$ Pa). Metal dissolution from the cycled LNMO electrode was estimated by measuring the Mn^{2+} and Ni^{2+} ion concentration in the electrolyte solution, and the metallic Ni and Mn that are deposited on the lithium negative electrode by inductively-coupled plasma (ICP) technique. For the latter analysis, the cycled lithium electrode was dissolved in a mixture of concentrated hydrochloric acid and nitric acid (3:1 in vol. ratio). Ac impedance measurement was made at the charged state (4.7 V) in the frequency range of 0.005 Hz–100 kHz with ac amplitude of 10 mV.

3. Results and discussion

It is known that LNMOs give slightly different XRD patterns depending on their chemical composition [16–18]. The stoichiometric $LiNi_{0.5}Mn_{1.5}O_4$ belongs to $P4_332$ space group (JCPDS #802184), in which the Ni^{2+} and Mn^{4+} ions are ordered in the 16d sites with 1:3 ratio. The non-stoichiometric (oxygen-deficient) $LiNi_{0.5}Mn_{1.5}O_{4-\delta}$, which are generated at higher calcination temperature or under more reducing condition, carry Mn^{3+} impurities that form to compensate the oxygen deficiency. The space group of this material is Fd3m (JCPDS #802162), wherein the transition metal ions are randomly distributed (disordered) in the 16d sites. As the positive electrode for lithium-ion batteries, the non-stoichiometric LNMO are known to outperform the stoichiometric one with respect to the cycle performance and rate capability, which can be ascribed to a superior electric conductivity that is resulted from the mixed-valency of Mn ions (co-existence of Mn^{3+} and Mn^{4+} ions) [17,19]. Fig. 1a shows the XRD pattern of the pristine LNMO powder. The stoichiometry of the pristine LNMO cannot be judged solely by the given XRD data since the stoichiometric and non-stoichiometric LNMO give only a marginal difference in their XRD patterns. Nonetheless, the used LNMO can be categorized as a non-stoichiometric one since the voltage profile shown in Fig. 1b provides a clear evidence for this. That is, the LNMO electrode exhibits a minor redox reaction around 4.0 V in addition to the major charge/discharge reaction at 4.6–4.7 V. The latter comes from the $Ni^{2+} \leftrightarrow Ni^{4+}$ redox reaction, whereas the former from the Mn^{3+} impurities ($Mn^{3+} \leftrightarrow Mn^{4+}$ redox reaction), which is the evidencing feature for the non-stoichiometry of LNMO [6,17]. Note that the stoichiometric LNMO shows only a redox reaction at 4.6–4.7 V (theoretical specific capacity = 148 mA h g^{-1}).

The high-temperature (60 °C) cycle performance of the LNMO electrode is presented in Fig. 2a along with the result obtained at 25 °C. The LNMO electrode shows a reasonable cycle performance at 25 °C. A stable cycle performance is observed even at 60 °C until 30 cycles, but a rapid capacity decay from the 40th cycle. The origin of capacity fading can be broadly classified into two; polarization loss and active material loss with cycling. The former is caused by the increase in either overpotential for electrode reactions or ohmic resistance including electrode resistance and electrolyte resistance.

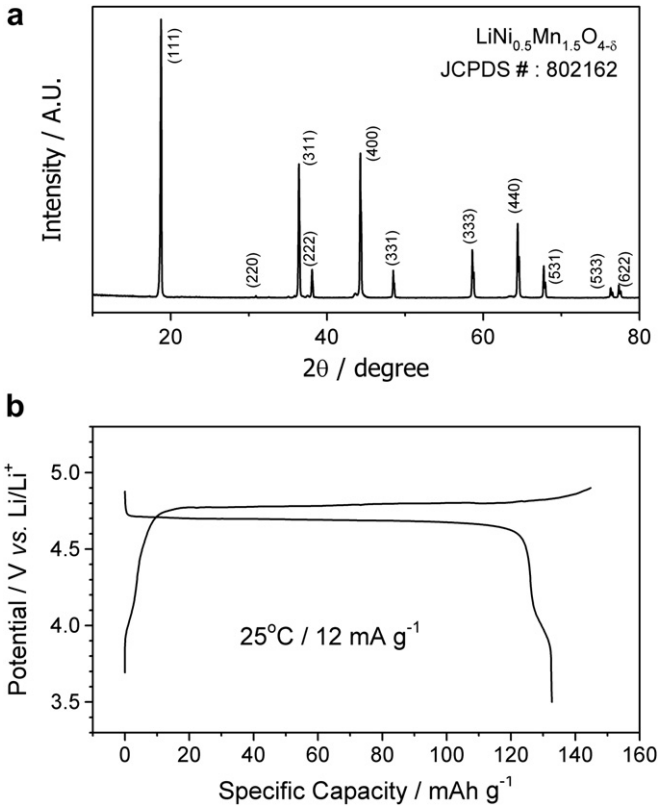

Fig. 1. X-ray diffraction pattern of $LiNi_{0.5}Mn_{1.5}O_{4-\delta}$ powder (a) and the galvanostatic charge/discharge voltage profile of Li/LNMO cell, which ensures that the LNMO sample is non-stoichiometric (b). Current density = 12 mA g^{-1}.

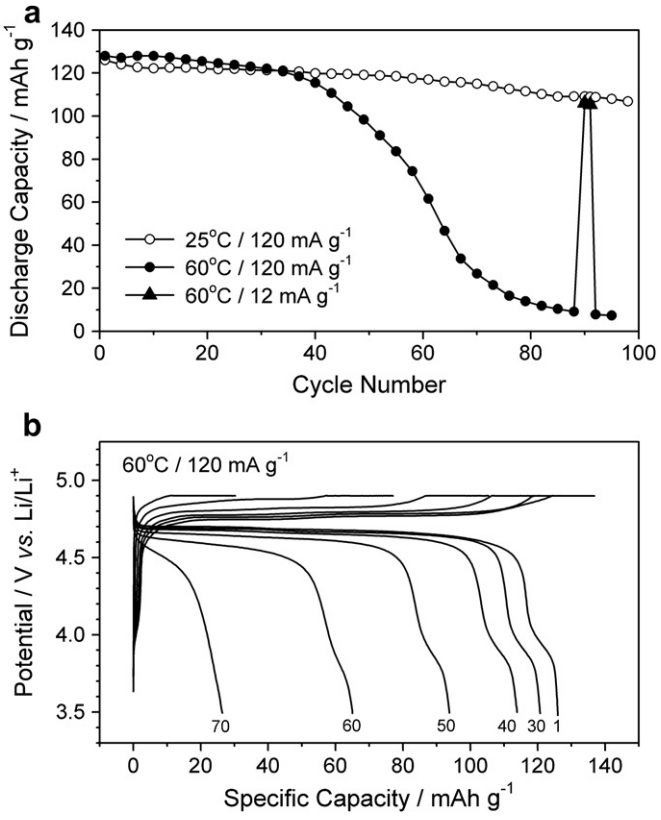

Fig. 2. Cycle performance of Li/LNMO cell at 25 °C and 60 °C (a). The galvanostatic charge/discharge voltage profiles obtained at 60 °C (b). Voltage cut-off = 3.5–4.9 V (*vs.* Li/Li^+). In (a), the current density was switched from 120 mA g^{-1} to 12 mA g^{-1} for the 90th ~ 92nd cycles and resumed back to 120 mA g^{-1} from the 93rd cycle.

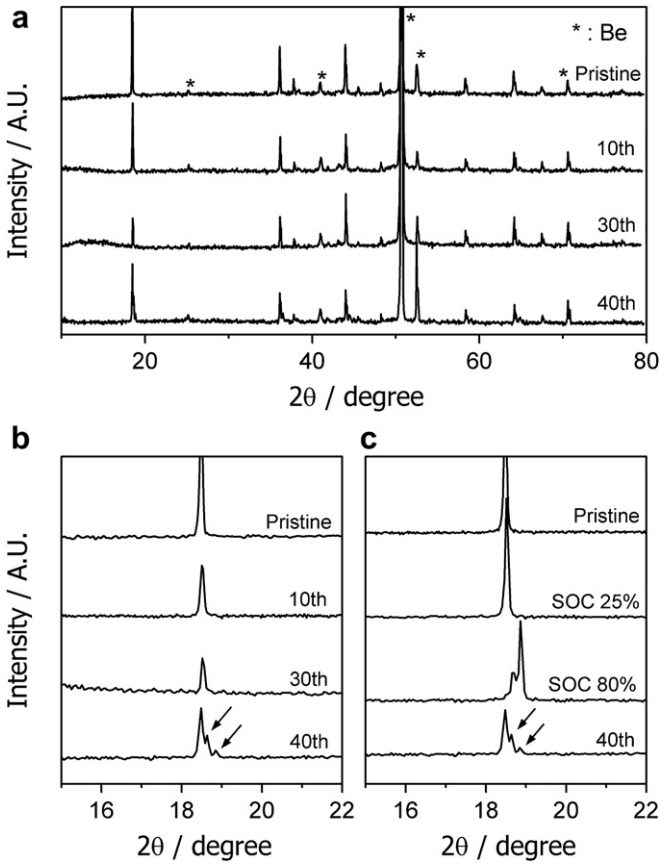

Fig. 3. X-ray diffraction patterns of $LiNi_{0.5}Mn_{1.5}O_4$ cycled at 60 °C (120 mA g^{-1}) (a). The XRD patterns were obtained at the discharge state (3.5 V) after the predetermined period of cycling. The magnified views of (111) diffraction peak (b). Note that additional (111) diffraction peaks (arrows) develop after 40 cycles. The (111) diffraction peaks for the LNMO samples of different state of charge (SOC) (c). The result obtained from the pristine sample (SOC = 0%) is also presented in (c).

The capacity loss caused by this origin is rate-dependent. That is, even if the capacity loss appears to be larger at a higher rate as a smaller capacity is delivered, the apparent capacity becomes larger when the charge/discharge rate is slowed down. The other origin for capacity fading is the loss of active material itself, which is frequently caused by dissolution of electrode active materials and/or irreversible structural change to inactive phases. In this case, the capacity cannot be recuperated even if the rate is slowed down since the material loss is irreversible. The latter possibility has been tested in this work by changing the galvanostatic charge/discharge rate. As shown in Fig. 2a, the Li/LNMO cell was cycled at 60 °C at a current density of 120 mA g^{-1} until the 89th cycle, during which the discharge capacity decays down to 10 mA h g^{-1}. When the current density is decreased from 120 mA g^{-1} to 12 mA g^{-1}, the discharge capacity appears as high as 110 mA h g^{-1}. Clearly, the capacity is recovered at a slower rate, reflecting that the irreversible material loss is insignificant. To conform this, the metal dissolution was measured after 80 cycles. The ICP analysis illustrates that 0.7% of Mn and 2.2% of Ni are dissolved from the cycled LNMO. The capacity loss, which is estimated from the dissolved Ni content, amounts to only 2.8 mA h g^{-1}. Surely, the material loss by metal dissolution is only marginal not to account for the severe capacity loss shown in Fig. 2a. Rather, the charge/discharge voltage profiles represented in Fig. 2b suggest that the capacity fading is associated with the ever-increasing electrode polarization. The electrode polarization estimated from the difference between the charge and discharge voltage becomes larger, particularly from the 40th cycle.

In order to see if the spinel LNMO phase is transformed to any inactive phases, the XRD patterns of cycled LNMO electrodes were examined (Fig. 3a). The XRD patterns of cycled LNMO electrodes are largely the same with that for the pristine one without any discernable diffraction peaks belonging to other than Fd3m space group. This illustrates that there are no structural transformations from the parent spinel to inactive phases during the high-temperature (60 °C) cycling. However, the magnified view of (111) diffraction peak reveals that additional peaks develop at the higher angle on the XRD pattern obtained after 40 cycles (Fig. 3b). To identify the new peaks, the XRD data of LNMO were obtained as a function of the state of charge (SOC). As shown in Fig. 3c, the (111) diffraction peak moves to the higher angle with an increase in the SOC [20]. The most intense (111) diffraction peak on the XRD pattern of the cycled electrode is matched with that for the pristine LNMO (SOC = 0%) (Fig. 3c), illustrating that almost of LNMO particles are fully discharged. This is not surprising since the XRD data were obtained after a full discharge. It is, however, clearly seen that the new peaks (arrows) are matched with those for the incompletely discharged samples (SOC of higher than zero), strongly suggesting that some of the LNMO particles are not fully discharged even if the electrode potential was moved down to 3.5 V in the final discharge period.

The incomplete discharging may be caused by electrical isolation of some LNMO particles in the composite electrode layer. This feature has been confirmed from the cross-sectional SEM images shown in Fig. 4. The cross-sectional image taken after 30 cycles shows that the composite electrode layer is still well-adhered to the Al current collector, and the electrode ingredients (LNMO and

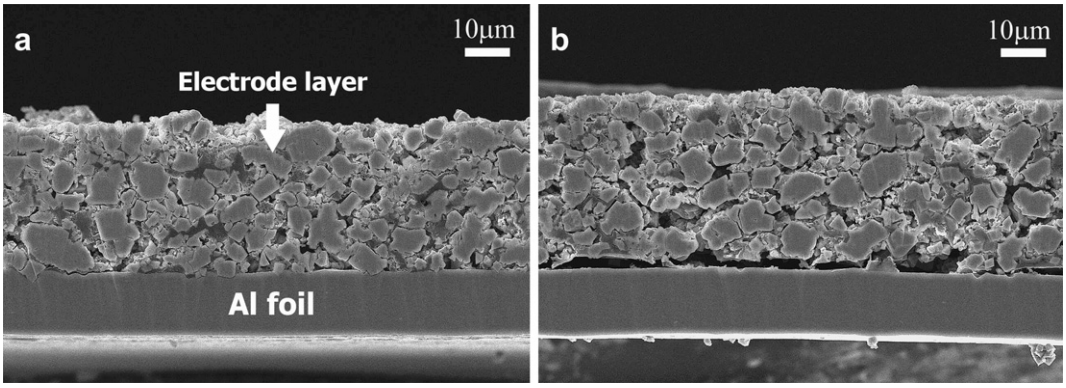

Fig. 4. Cross-sectional views of LNMO composite electrodes; after 30 cycles (a) and 40 cycles (b) at 60 °C. Current density = 120 mA g^{-1}.

carbon particles) make an intimate contact to each other (Fig. 4a). The image taken after 40 cycles (Fig. 4b) reveals that the composite electrode layer is swollen and the cracks develop at the interface of the electrode layer and Al foil, and also inside the composite electrode layer. Note that the FE-SEM image could not be obtained with the 60 times cycled electrode since the electrode layer has already been peeled off from Al foil. This FE-SEM result can account for the electrode polarization (Fig. 2b) and incomplete discharging of LNMO (Fig. 3b), both of which become significant from about 40th cycle. That is, the contact loss at the electrode layer/Al foil interface and between the LNMO (carbon)/LNMO (carbon) particles inside the electrode layer leads to an increase in the electrode resistance, which eventually leads to the electrode polarization. Also, due to electrical isolation, some LNMO particles are not active any more for charge/discharge reaction.

Electrode swelling and contact losses are frequently observed with some negative electrodes that suffer from a massive volume change with cycling; the Li-alloying materials such as Si and Sn [21–24], and the metal oxides that are lithiated by conversion reaction [10,25]. As far as the positive electrode materials are concerned, the volume change is not serious. For instance, it is known that the spinel $LiMn_2O_4$ shows only below 3% of volume change upon charge and discharge [26]. It is thus very likely that the volume change cannot account for the contact loss observed with the spinel-structured LNMO in this work. Rather, it is intuitive that the decomposition of cell constituents is serious under such a highly oxidizing condition (high-voltage up to 4.9 V and elevated temperature) and this may lead to the contact losses. Here, many scenarios can be assumed. Namely, if any film is deposited as a result of electrolyte decomposition between the LNMO (or carbon) particles, some of LNMO particles can be electrically isolated since the electrolyte-derived films are electrically insulating. The acid generation (for instance, HF) as a result of electrolyte decomposition can also be assumed [27], which may attack the Al foil, LNMO, and polymeric binder. Oxidative decomposition of the binder and carbon can also lead to contact losses [28]. A systematic study is needed to identify the most dominant failure mechanism among those.

In this work, several countermeasures were made to improve the cycle performances of LNMO electrode at elevated temperature (Fig. 5). When the plain Al foil is replaced by the etched one, the cell degradation is slightly mitigated, which must be due to a better adhesion of the electrode layer to the etched Al foil. A similar improvement is observed by loading a larger amount of binder (PVdF, 10 wt. %). The cell performance is further improved by increasing the load of carbon (Denka black) and binder. The electrode polarization was compared for two LNMO composite electrodes by taking ac impedance spectra (Fig. 6). As seen in Fig. 6,

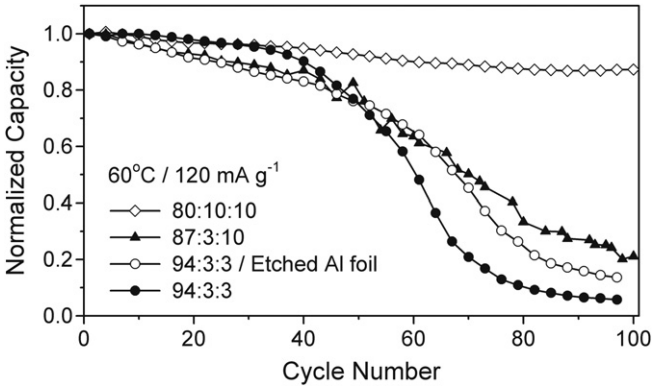

Fig. 5. Cycle performance of Li/LNMO cell with a variation either in the electrode composition (wt. % of LNMO, Denka black and PVdF) or Al current collector.

both electrodes show an impedance increase with cycling. The composite electrode containing a larger amount of carbon and binder (LNMO; Denka black: PVdF = 80:10:10 in wt. %), which shows a better cycle performance in Fig. 5, exhibits a rather modest impedance increase. However, the other one fabricated with a lesser amount of carbon and binder (94:3:3) exhibits a drastic increase, in particular between the 35th and 55th cycle. This is consistent with the cycling data (Fig. 5), in which a rapid capacity decay is noted from the 40th cycle. This ensures that the electrode failure is deeply associated with electrode polarization. In short, both high population of conductive carbon particles and strong binding force given by the binder are needed to minimize the electric contact loss and to achieve a satisfactory cycle performance under a highly oxidizing condition.

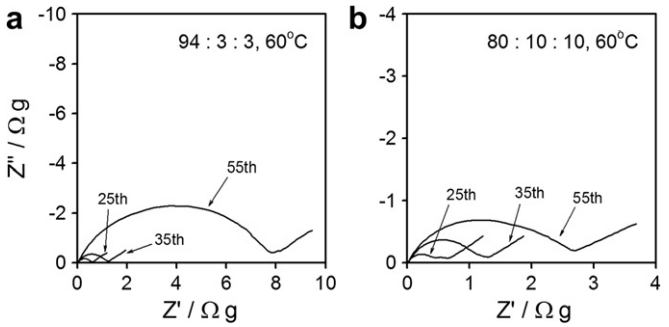

Fig. 6. Evolution of cell impedance upon cycling observed with two composite electrodes. The composition (wt. % of LNMO, Denka black and PVdF) for two electrodes is: (a); 94:3:3 and (b); 80:10:10.

4. Conclusion

The failure mechanism of 5 V $LiNi_{0.5}Mn_{1.5}O_4$ electrode at elevated temperature was studied. The metal dissolution was not serious. XRD result shows that the phase transition from spinel to other inactive phases is not likely. The dominant failure mechanism turned out to be the contact loss at both the electrode/current collector interface and between the LNMO (carbon) particles. Such contact losses lead to an increase in the electrode resistance and eventually a capacity fading as a result of electrode polarization. The contact loss inside the electrode layer generates some isolated LNMO particles that are no more active for charge and discharge reaction. The countermeasures to reinforce the electrically conductive network can mitigate the electrode failure.

Acknowledgments

This work was supported by the MEST through the WCU program (R31-10013) and NRF-2010-C1AAA001-2010-0029065.

References

[1] M.M. Thackeray, C.S. Johnson, J.T. Vaughey, H.N. Li, S.A. Hackney, J. Mater. Chem. 15 (2005) 2257.
[2] C.S. Johnson, N. Li, C. Lefief, J.T. Vaughey, M.M. Thackeray, Chem. Mater. 20 (2008) 6095.
[3] J. Hong, D.-H. Seo, S.-W. Kim, H. Gwon, S.-T. Oh, K. Kang, J. Mater. Chem. 20 (2010) 10179.
[4] D. Kim, S. Park, O.B. Chae, J.H. Ryu, Y.-U. Kim, R.-Z. Yin, S.M. Oh, J. Electrochem. Soc. 159 (2012) A193.
[5] T. Ohzuku, S. Takeda, M. Iwanaga, J. Power Sources 81-82 (1999) 90.
[6] Y. Terada, K. Yasaka, F. Nishikawa, T. Konishi, M. Yoshio, I. Nakai, J. Solid State Chem. 156 (2001) 286.
[7] J. Mun, T. Yim, K. Park, J.H. Ryu, Y.G. Kim, S.M. Oh, J. Electrochem. Soc. 158 (2011) A453.
[8] D.H. Jang, Y.J. Shin, S.M. Oh, J. Electrochem. Soc. 143 (1996) 2204.
[9] L. Yunjian, L. Xinhai, G. Huajun, W. Zhixing, H. Qiyang, P. Wenjie, Y. Yong, J. Power Sources 189 (2009) 721.
[10] Y.K. Sun, K.J. Hong, J. Prakash, K. Amine, Electrochem. Commun. 4 (2002) 344.
[11] R. Kostecki, F. McLarnon, Electrochem. Solid State Lett. 7 (2004) A380.
[12] Y. Talyosef, B. Markovsky, G. Salitra, D. Aurbach, H.J. Kim, S. Choi, J. Power Sources 146 (2005) 664.
[13] S.-T. Myung, Y. Hitoshi, Y.-K. Sun, J. Mater. Chem. 21 (2011) 9891.
[14] B. Markovsky, Y. Talyossef, G. Salitra, D. Aurbach, H.-J. Kim, S. Choi, Electrochem. Commun. 6 (2004) 821.
[15] D. Aurbach, B. Markovsky, Y. Talyossef, G. Salitra, H.-J. Kim, S. Choi, J. Power Sources 162 (2006) 780.
[16] C.M. Julien, F. Gendron, A. Amdouni, M. Massot, Mater. Sci. Eng.: B 130 (2006) 41.
[17] M. Kunduraci, G. Amatucci, Electrochim. Acta 53 (2008) 4193.
[18] T.-F. Yi, Y. Xie, M.-F. Ye, L.-J. Jiang, R.-S. Zhu, Y.-R. Zhu, Ionics 17 (2011) 383.
[19] J.H. Kim, S.T. Myung, C.S. Yoon, S.G. Kang, Y.K. Sun, Chem. Mater. 16 (2004) 906.
[20] M. Kunduraci, G.G. Amatucci, J. Electrochem. Soc. 153 (2006) A1345.
[21] H. Robert, J. Power Sources 81–82 (1999) 13.
[22] C.J. Wen, R.A. Huggins, J. Electrochem. Soc. 128 (1981) 1181.
[23] M. Winter, R.J. Brodd, Chem. Rev. 104 (2004) 4245.
[24] S.-C. Chao, Y.-C. Yen, Y.-F. Song, Y.-M. Chen, H.-C. Wu, N.-L. Wu, Electrochem. Commun. 12 (2010) 234.
[25] J. Cabana, L. Monconduit, D. Larcher, M.R. Palacín, Advan. Mater. 22 (2010) E170.
[26] Y. Shin, A. Manthiram, J. Electrochem. Soc. 151 (2004) A204.
[27] Y. Talyosef, B. Markovsky, R. Lavi, G. Salitra, D. Aurbach, D. Kovacheva, M. Gorova, E. Zhecheva, R. Stoyanova, J. Electrochem. Soc. 154 (2007) A682.
[28] L. Fransson, T. Eriksson, K. Edström, T. Gustafsson, J.O. Thomas, J. Power Sources 101 (2001) 1.